Array Element Localization Accuracy and Survey Design

Stan E. Dosso[1] and Gordon R. Ebbeson[2]

[1]School of Earth and Ocean Sciences, University of Victoria, Victoria BC Canada V8W 3Y2

[2]Defence Research & Development Canada–Atlantic, P.O. BOX 1012 Dartmouth NS Canada B2Y 3Z71

ABSTRACT

Accurate localization of the individual elements of an underwater acoustic receiver array is an important prerequisite to advanced array processing applications. Array element localization (AEL) methods are typically based on inverting acoustic arrival-time measurements from controlled sources at (approximately) known positions to the receivers to be localized. This paper presents and illustrates a general approach to AEL inversion and to AEL survey design based on quantifying the posterior receiver-location uncertainty, taking into account uncertainties in the data, source locations, sound speed, and water depth. The inversion is based on a fast ray-tracing algorithm that employs Newton's method and the method of images to determine eigenrays for direct and reflected arrivals. The efficiency of this approach allows computationally intensive analysis such as Monte-Carlo appraisal and nonlinear optimization for designing optimal source configurations. These algorithms provide a rigorous approach that can be applied to examine all aspects of AEL accuracy and survey design, illustrated here by several examples. It is shown that synchronized AEL surveys (in which source transmission times are known) provide only a minor improvement over non-synchronized surveys (often much simpler logistically), and the difference can be made up by using more sources in an optimal configuration or by including additional arrivals. Including multiple-reflected arrivals improves receiver depth estimates (provided water depth is well known), but provides little improvement in horizontal localization.

SOMMAIRE

La localisation précise d'éléments individuels d'un étalage de récepteurs acoustiques sous-marin est un facteur important qui peut fortement influencer la validité de la manipulation de données. Les methodes de Localisation des Eléments d'Etalage (AEL) sont typiquement basées sur l'inversion de temps d'arivée acoustiques mesurés, parvenant de sources contr ōlées à des positions connues (approximativement), relatives aux positions des récepteurs localiser. Cet article présente et illustre une approche gnérale à l'inversion de AEL et à la planifications d'études de AEL, basée sur la quantification de l'incertitude postérieure de la position des récepteurs, compte-tenue de l'incertitude des données, de la position des sources, de la vitesse sonore, et de la profondeur d'eau. L'inversion est basée sur un algorithme rapide de traage de rayon qui utilise la méthode Newton et la méthode d'images pour déterminer les rayons-eigen pour les arives directes et reflétées. L'efficacité de cette approche permet l'utilisation de méthodes calcul informatique intense, comme l'évaluation Monte-Carlo et l'optimisation non-linéaire, pour la planification de configuration de sources optimale. Ces algorithmes fournissent une approche qui peut étre applique pour examiner tout les aspects de la précision et de la planification d'études de AEL, illustré ici par plusieurs exemples. Il est démontr ici que les études de AEL harmonisés (pour qui les temps de transmission de source sont connues) fournissent seulement une amélioration mineure comparativement aux études non-harmonizés (qui ont souvent une logistique plus simple), et que la différence peut étre rcupre en utilisant plus de sources dans une configuration optimale ou en incluant des arivées additionnelles. En incluant les arivées à réflextion multiple, l'estimation de profondeur des récepteurs est améliore (à condition que la profondeur d'eau est bien connue), mais n'améliore que peu la localisation horizontale.

1. INTRODUCTION

Array processing methods in underwater acoustics require accurate knowledge of the locations of individual elements in a receiver array [1,2]. However, sufficiently accurate receiver locations are often not know after array deployment at sea, and array element localization (AEL) surveys are typically required. AEL is based on inverting acoustic arrival-time measurements from a series of controlled sources to the receivers to be localized. AEL methods usually use direct acoustic-path arrivals, but can also include surface- and/or bottom-reflected arrivals to provide more information, provided these arrivals can be identified. Synchronized AEL surveys (in which the source transmission instants are known and the data rep-

resent absolute travel times) are often more complicated logistically than non-synchronized surveys (which provide relative travel times), but produce more informative data. A third possibility is that of synchronized surveys which make use of cross-correlation or waveform envelope techniques to pick arrival times, and hence provide data consisting of absolute travel times but with an unknown offset that is common for all data.

Ideally, AEL inversion should address all (significant) sources of error in the acoustic survey, and incorporate physical prior information about the solution in addition to the measured data. Although the source positions are often treated as known parameters in AEL inversion, in reality, errors in these positions are often significant and represent the limiting factor [3]. This limitation can be addressed using the method of regularization to formulate an inversion that properly treats both source and receiver positions as unknown parameters with prior estimates and associated uncertainties [3–10]. An unknown bias to the measured sound-speed profile (commonly due to inexact calibration [11]) can also be included in the inversion. For arrays that are expected to be essentially straight, a regularization can be formulated for the smoothest array shape (i.e., the shape with minimum curvature or changes in direction) subject to fitting the acoustic data to a statistically appropriate level. Regularized inversion has been applied to diverse AEL problems involving fixed horizontal arrays [3–5], moored vertical arrays [5, 6], towed arrays [7, 8], and freely-drifting sonobuoy fields [9, 10].

The uncertainties of the recovered receiver positions can be estimated efficiently from a linearized approximation of the posterior covariance matrix, evaluated at the regularized solution. Alternatively, uncertainty estimates can be derived from a Monte Carlo appraisal procedure which calculates sensor-location error statistics from an ensemble of noisy synthetic inversion results [3]. Monte Carlo appraisal is computationally intensive, but represents a fully nonlinear solution, and also can be formulated to provide relative receiver position uncertainties by correcting each inversion result for optimal translation and rotation (linearized uncertainty estimates represent absolute uncertainties). Regularized AEL inversion and Monte Carlo appraisal, including the associated assumptions regarding data error statistics (described in Sec. 3), have been verified by comparing AEL results to a high-precision optical survey for a 2-D array, including both horizontal and vertical sub-arrays, deployed from shore-fast Arctic sea ice [5].

The geometric configuration of acoustic sources is an important factor controlling the accuracy of AEL inversion: a good configuration can provide much more accurate AEL results than a poor configuration [12]. The optimal source configuration can be determined for a particular array deployment by minimizing the mean receiver localization error over source positions. This represents a challenging numerical optimization problem, and, for efficiency, the localization error is based on the linearized estimate. Computing optimal source configurations also allows various aspects of AEL inversion, such as the effect of the number of sources, to be examined in a meaningful manner.

AEL inversion is based on inverting the acoustic ray-tracing equations. Hence, efficient AEL algorithms require an efficient ray-tracer; this is particularly important for the computationally-intensive Monte Carlo and optimization applications. The ray-tracer developed here is designed to determine eigenrays (rays that connect source and receiver) using Newton's method to iteratively improve an initial estimate. Since AEL surveys are based on simple, specific acoustic paths, this approach is much more efficient than than standard methods of shooting a large number of rays to bracket (trap) and subsequently refine eigenrays. Newton's method is applied to surface- and/or bottom-reflected rays using the method of images.

The remainder of this paper is organized as follows. The ray-tracing algorithm is described in Section 2. Section 3 develops the regularized AEL inversion and linearized uncertainty estimation. Section 4 describes the Monte Carlo appraisal for nonlinear uncertainty estimation. Section 5 considers design of optimal AEL source configurations. A synthetic example illustrating AEL inversion/uncertainty estimation and considering several factors affecting AEL accuracy and survey design runs through these sections. Finally, Section 6 summarizes and discusses this work. This paper is the result of a recent project to unify and extend previous disparate work in AEL [3–10, 12]. Hence, while portions of the theory in Sections 3–5 have been presented elsewhere, this paper is the first to provide a complete, systematic, and self-consistent approach to the various AEL applications (and also corrects several earlier errors). Further, the extension of the efficient ray-tracer and AEL inversion to reflected and turning ray paths and the applications to study AEL accuracy and survey design are novel.

2. RAY TRACING

Consider an ocean acoustic source and receiver at $(x_j,\, y_j,\, z_j)$ and $(x_i,\, y_i,\, z_i)$, respectively, with $z_j \le z_i$ (source above receiver is assumed here; for the opposite, a negative sign is required in the integrals below unless otherwise noted). The horizontal range between source and receiver is given by

$$r = \left[(x_i - x_j)^2 + (y_i - y_j)^2\right]^{1/2} . \tag{1}$$

Expressions for the range r and arrival-time t between source and receiver along a non-turning direct ray (i.e., a ray that does not change vertical direction as the result of reflection or refraction) are obtained by applying Snell's Law to an infinite stack of infinitesimal layers [13]

$$r = \int_{z_j}^{z_i} \frac{p\, c(z)\, dz}{\left[1 - p^2 c^2(z)\right]^{1/2}} , \tag{2}$$

$$t = t_0 + \int_{z_j}^{z_i} \frac{dz}{c(z)\left[1 - p^2 c^2(z)\right]^{1/2}} , \tag{3}$$

where t_0 represents the source transmission time. In Eqs. (2) and (3), the ray parameter $p = cos\theta(z)/c(z)$

(where $\theta(z)$ is the grazing angle) is invariant along a ray path, and defines the take-off angle at the source. The ray parameter for an eigenray connecting source and receiver is determined by searching for the value of p which produces the correct range (to a specified tolerance) using Eq. (2). The efficiency of this search is the key to an efficient ray-tracing algorithm.

For non-turning direct-path eigenrays, a highly efficient procedure of determining p is based on Newton's method. An initial estimate p_0 is based on straight-line propagation with a constant sound speed c_H representing the harmonic mean of the water-column sound-speed profile between source and receiver

$$c_H = (z_i - z_j) \Bigg/ \int_{z_j}^{z_i} \frac{dz}{c(z)} \tag{4}$$

(this equations also holds for $z_i \leq z_j$). An improved estimate p_1 is obtained by expanding $r(p)$ in a Taylor's series about p_0 and neglecting nonlinear terms leading to

$$p_1 = p_0 + \left[\frac{\partial r(p_0)}{\partial p}\right]^{-1} (r(p) - r(p_0)) \,. \tag{5}$$

In Eq. (5), $\partial r/\partial p$ is determined by differentiating (2) according to Leibnitz's rule to yield

$$\frac{\partial r}{\partial p} = \int_{z_j}^{z_i} \frac{c(z)\, dz}{[1 - p^2 c^2(z)]^{3/2}} \,. \tag{6}$$

If $r(p_1)$ computed from Eq. (2) is within the tolerance of the desired range according to Eq. (1), the procedure is complete. If not, the starting value is updated, $p_0 \leftarrow p_1$, and the procedure repeated iteratively until a satisfactory value is obtained. Since Newton's method converges quadratically near the solution, this is a highly efficient method of determining eigenrays to high precision, often requiring only one or two iterations. Once the ray parameter p is determined, the travel-time along the ray path is computed using Eq. (3).

In addition to computing travel times, AEL inversion (described in Section 3) requires partial derivatives of travel-time with respect to source and receiver coordinates, source instants, and sound-speed bias. Consider first the partial derivative with respect to horizontal coordinate x_i. Employing the chain rule

$$\frac{\partial t}{\partial x_i} = \frac{\partial t}{\partial p}\frac{\partial p}{\partial r}\frac{\partial r}{\partial x_i} = \frac{\partial t}{\partial p}\left[\frac{\partial r}{\partial p}\right]^{-1}\frac{\partial r}{\partial x_i} \,. \tag{7}$$

The three partials on the right side of Eq. (7) can be calculated from Eqs. (3), (2) and (1), respectively, yielding

$$\frac{\partial t}{\partial x_i} = p\,(x_i - x_j)/r \,. \tag{8}$$

Similarly, partial derivatives with respect to the other horizontal coordinates are

$$\frac{\partial t}{\partial x_j} = p\,(x_j - x_i)/r \,, \tag{9}$$

$$\frac{\partial t}{\partial y_i} = p\,(y_i - y_j)/r \,, \tag{10}$$

$$\frac{\partial t}{\partial y_j} = p\,(y_j - y_i)/r \,. \tag{11}$$

The partial derivative of t with respect to vertical coordinate z_i can be determined from Eq. (3)

$$\frac{\partial t}{\partial z_i} = \int_{z_j}^{z_i} \frac{p\, c(z)\, dz}{[1 - p^2 c^2(z)]^{3/2}} \left(\frac{\partial p}{\partial z_i}\right) - \frac{1}{c(z_i)\,[1 - p^2 c^2(z_i)]^{1/2}} \,. \tag{12}$$

An expression for $\partial p/\partial z_i$ can be obtained by noting that

$$\frac{\partial r}{\partial z_i} = 0 = \int_{z_j}^{z_i} \frac{c(z)\, dz}{[1 - p^2 c^2(z)]^{3/2}} \left(\frac{\partial p}{\partial z_i}\right) - \frac{p\, c(z_i)}{[1 - p^2 c^2(z_i)]^{1/2}} \,. \tag{13}$$

Solving for $\partial p/\partial z_i$ and substituting into Eq. (12) yields

$$\frac{\partial t}{\partial z_i} = \frac{1}{c(z_i)}\left[1 - p^2\, c^2(z_i)\right]^{1/2} \,. \tag{14}$$

Similarly,

$$\frac{\partial t}{\partial z_j} = -\frac{1}{c(z_j)}\left[1 - p^2 c^2(z_j)\right]^{1/2} \,. \tag{15}$$

The derivative of t with respect to the source instant t_0 in Eq. (3) is simply given by

$$\frac{\partial t}{\partial t_0} = 1. \tag{16}$$

However, for the purposes of AEL inversion, t_0 in Eq. (3) is replaced by $(\bar{c}t_0)/\bar{c}$, where $\bar{c}$ represents a representative sound speed. This allows the unknown source instant to be represented as $\bar{c}t_0$, which has the same physical units (distance) and similar uncertainty as the positional parameters (scaling parameters in this manner generally improves the numerical stability of inversion algorithms). In this case the partial derivative becomes

$$\frac{\partial t}{\partial(\bar{c}t_0)} = \frac{1}{\bar{c}} \,. \tag{17}$$

Measured sound-speed profiles are generally accurate in a relative sense, but frequently suffer from bias errors of up to 2 m/s due to inaccurate calibration [11]. To account for an unknown bias in the sound-speed profile, let $c(z) = c_t(z) + c_b$, where $c_t(z)$ is the true sound speed and c_b is the bias. Differentiating Eq. (3) with respect to c_b (and noting $\partial p/\partial c = -p/c$) leads to

$$\frac{\partial t}{\partial c_b} = -\int_{z_j}^{z_i} \frac{dz}{c^2(z)\,[1 - p^2 c^2(z)]^{1/2}} \,. \tag{18}$$

Sea surface and bottom reflections can be included in the above formulation for direct rays using the method of images, i.e., by representing the reflected ray path by

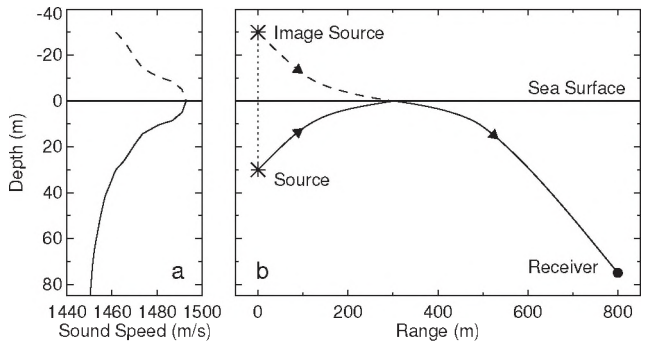

Figure 1: Example of tracing a surface-reflected ray using the method of images. Panel (a) shows the "image" sound-speed profile, with structure reflected about the sea surface. Panel (b) shows the equivalence of a reflected path and a direct path traced through the image sound-speed profile.

a direct path from an image source located above the surface or below the bottom, respectively. To apply the method of images, the sound-speed profile is reflected about the interface in the same manner as the source, and a direct ray is traced through the resulting "image" sound-speed profile. An example of this procedure is illustrated in Fig. 1 for a surface-reflected ray. Ray paths involving multiple reflections can be accommodated by applying the method of images recursively.

To implement the equations derived above, it is assumed that a discrete sound-speed profile can be represented by a series of layers with a (non-zero) linear gradient in each layer. In the following, let $\{(z_k, c_k), k = 1, N_z\}$ represent the piece-wise linear sound-speed profile (including any required profile reflections), and let $\{g_k\}$ be the corresponding sound speed gradients. The integrals in Eqs. (2), (3), (4), (6), and (18) can be evaluated analytically, yielding the following results, where $w_k \equiv (1 - p^2 c_k^2)^{1/2}$,

$$r = \sum_{k=j}^{i-1} \frac{w_k - w_{k+1}}{p\, g_k}, \tag{19}$$

$$t = t_0 + \sum_{k=j}^{i-1} \frac{1}{g_k} \left[\log_e \frac{c_{k+1}\,(1 + w_k)}{c_k\,(1 + w_{k+1})} \right], \tag{20}$$

$$c_H = (z_i - z_j) \Bigg/ \sum_{k=j}^{i-1} \frac{1}{g_k} \left[\log_e \frac{g_k(z_{k_1} - z_k) + c_k}{c_k} \right], \tag{21}$$

$$\frac{\partial r}{\partial p} = \sum_{k=j}^{i-1} \frac{w_k - w_{k+1}}{p^2\, g_k\, w_k\, w_{k+1}}, \tag{22}$$

$$\frac{\partial t}{\partial c_b} = \sum_{k=j}^{i-1} \frac{1}{g_k} \left[\frac{w_{k+1}}{c_{k+1}} - \frac{w_k}{c_k} \right]. \tag{23}$$

If a non-turning eigenray cannot be found for a particular source/receiver depth and range, a search over turning rays is required. An efficient strategy for this search uses the average sound-speed gradient between source and receiver as an indicator of the most likely take-off direction for a turning ray. Given $z_j < z_i$ (source above receiver), consider first the case of a negative (downward-refracting) average gradient. In this case, the first rays considered are those leaving the source upward to see if they turn back down to the receiver. This is accomplished efficiently by considering rays that turn at the top of each layer of the sound-speed profile above the source. If $g_k < 0$, the p value for an upward propagating ray turning at the top of the kth layer is given by

$$p = 1/c_k. \tag{24}$$

If tracing rays that turn at successive layer boundaries bracket the receiver, an eigenray is trapped and can be refined using the bisection method. If no such eigenrays exists, a secondary search can be carried out over downward-propagating rays that turn upward below the receiver (if such rays exist) using a similar strategy. Alternatively, if the average sound-speed gradient between source and receiver is positive (upward-refracting), the initial search is over rays that turn upward at layer boundaries below the receiver, followed by rays that turn downward above the source (if they exist). The above strategy is used for $z_j > z_i$ (receiver above source) by applying reciprocity.

Once the ray parameter p is determined for a turning ray, the integrals along the ray-path are evaluated. Consider, for example, the case of an initially downward propagating ray entering the lth layer with a positive sound-speed gradient g_l. The turning depth for this ray is given by

$$z_T = z_l + (1/p - c_l)/g_l. \tag{25}$$

If this depth is less than z_{l+1} (bottom of lth layer) the ray turns in this layer; if not, it proceeds into layer $l+1$. If the ray turns in layer l, then the integration involves four steps: (i) integrate from the source depth z_j down to z_l, (ii) integrate from z_l to z_T (where $w_T = 0$), (iii) integrate upward from z_T to z_l, and (iv) integrate from z_T to the receiver depth z_i. This leads to the following equations for turning rays:

$$r = \sum_{k=j}^{l-1} \frac{w_k - w_{k+1}}{p\, g_k} + \frac{2\, w_l}{p\, g_l} + \sum_{k=l}^{i} \frac{w_k - w_{k-1}}{p\, g_{k-1}}, \tag{26}$$

$$\begin{aligned} t \;=\; & t_0 + \sum_{k=j}^{l-1} \frac{1}{g_k} \left[\log_e \frac{c_{k+1}\,(1 + w_k)}{c_k\,(1 + w_{k+1})} \right] + \frac{2}{g_l} \log_e \frac{1 + w_l}{p\, c_l} \\ & + \sum_{k=l}^{i} \frac{1}{g_{k-1}} \left[\log_e \frac{c_{k-1}\,(1 + w_k)}{c_k\,(1 + w_{k-1})} \right], \end{aligned} \tag{27}$$

$$\begin{aligned} \frac{\partial r}{\partial p} \;=\; & \sum_{k=j}^{l-1} \frac{w_k - w_{k+1}}{p^2\, g_k\, w_k\, w_{k+1}} - \frac{2}{g_l\, p^2\, w_l} \\ & + \sum_{k=l}^{i} \frac{w_k - w_{k-1}}{p^2\, g_{k-1}\, w_k\, w_{k-1}}, \end{aligned} \tag{28}$$

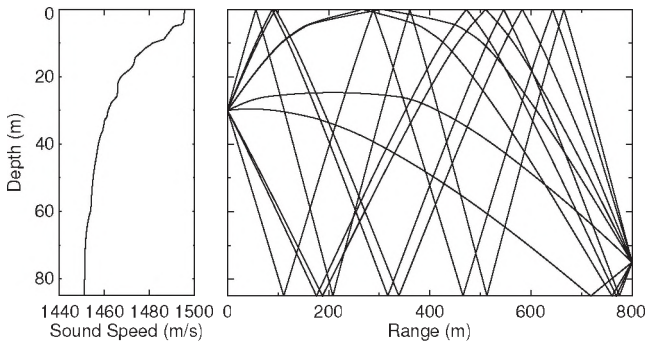

Figure 2: Ray-tracing example. Left panel shows downward-refracting sound-speed profile. Right panel shows ray paths for direct ray and all reflected rays with up to two bottom reflections (ten paths).

$$\frac{\partial t}{\partial c_b} = \sum_{k=j}^{l-1} \frac{1}{g_k}\left[\frac{w_{k+1}}{c_{k+1}} - \frac{w_k}{c_k}\right] + \frac{2\,w_l}{c_l g_l} + \sum_{k=l}^{i} \frac{1}{g_{k-1}}\left[\frac{w_{k-1}}{c_{k-1}} - \frac{w_k}{c_k}\right]. \quad (29)$$

Similar equations can be derived for an initially upward propagating ray that turns in a negative sound-speed gradient.

An example of the above ray-tracing algorithm is given in Fig. 2 for a challenging case involving a strongly downward refracting sound-speed profile with variable gradients and a near-surface mixed (near iso-speed) layer. The water depth is 85 m and the source and receiver depths are 30 and 75 m, respectively. Figure 2 shows all rays with up to three surface and two bottom reflections for a range of 800 m. The direct and bottom-reflected rays are turning rays which require the bisection search to determine the corresponding ray parameters. All other rays were determined using Newton's method. The surface- and surface-bottom reflected rays are close to turning near the ocean surface (i.e., go through small grazing angles); this represents a difficult ray-parameter search and required 8 iterations of Newton's method to converge to a range tolerance of 0.01 m. All other rays required only two iterations for convergence.

3. AEL INVERSE THEORY

The AEL inverse problem formulated here consists of estimating 3-D position variables (x, y, z) for the N_r receivers and N_s sources of an AEL survey, based on linearized inversion of travel-time data as represented by the acoustic ray theory developed in Section 2. The data can include direct and/or surface- and bottom-reflected arrivals, and can consist of absolute travel times (known source transmission instants), relative travel times (unknown source instants), or absolute travel times with an unknown offset. In the case of relative travel times, N_s source instants are included as explicit unknown parameters in the inversion. For travel-time data with an unknown transmission offset, the offset is included as a single parameter. Finally, the bias for the measured sound-speed profile is also considered as an unknown parameter in the inversion.

The acoustic arrival times $\mathbf{t}$ measured in an AEL survey can be written in general vector form as

$$\mathbf{t} = \mathbf{t}(\mathbf{m}) + \mathbf{n}. \quad (30)$$

In Eq. (30), the model $\mathbf{m}$ represents the unknown parameters (discussed above). The forward mapping $\mathbf{t}(\mathbf{m})$ represents computation of acoustic arrival times along ray paths between sources and receivers. Finally, $\mathbf{n}$ represents additive errors (noise), with the assumption that the error n_i on datum t_i is due to an independent, Gaussian-distributed random process with zero mean and standard deviation σ_i.

The inverse problem of estimating $\mathbf{m}$ from $\mathbf{t}$ is functionally nonlinear. However, a local linearization can be obtained by expanding $\mathbf{t}(\mathbf{m}) = \mathbf{t}(\mathbf{m_0}+\delta\mathbf{m})$ in a Taylor series to first order about an arbitrary starting model $\mathbf{m_0}$ leading to [3]

$$\mathbf{J}\,\mathbf{m} = \mathbf{t} - \mathbf{t}(\mathbf{m_0}) + \mathbf{J}\,\mathbf{m_0} \equiv \mathbf{d}, \quad (31)$$

where $\mathbf{J}$ is the Jacobian matrix of partial derivatives $J_{ij} = \partial t_i(\mathbf{m_0})/\partial m_j$ (derived in Section 2), and $\mathbf{d}$ represents modified data defined in terms of known quantities. Equation (31) represents a linear inverse problem which can be solved for $\mathbf{m}$ as described below. Since nonlinear terms are neglected, the linearized inversion must be repeated iteratively until convergence.

Treating both source and receiver locations as unknown leads to an ill-conditioned inverse problem which cannot be solved using standard least-squares methods even in cases where the number of data exceed the number of unknowns. This ill-conditioning indicates that the data alone do not constrain the solution, and additional independent information (prior information) is required. The method of regularization [14–16] provides a powerful approach to include prior information in linear inversion. This is accomplished by minimizing an objective function ϕ that combines the data misfit with regularizing terms that impose the prior information. Two forms of prior information are typically available in AEL problems, and can be imposed by including two regularization terms:

$$\phi = |\mathbf{G}\,(\mathbf{J}\,\mathbf{m} - \mathbf{d})|^2 + \mu_1|\mathbf{H}_1\,(\mathbf{m} - \hat{\mathbf{m}}_1)|^2 + \mu_2|\mathbf{H}_2\,(\mathbf{m} - \hat{\mathbf{m}}_2)|^2. \quad (32)$$

In (32), the first term represents the (linearized) χ^2 data misfit, and the remaining terms represent regularizations (described below) with trade-off parameters (Lagrange multipliers) μ_1 and μ_2 determining the relative importance of the three terms in the minimization.

The first regularization term in Eq. (32) applies prior parameter estimates for the source and receiver positions as available from knowledge of the deployment procedure. Hence, $\hat{\mathbf{m}}_1$ consists of the prior estimates for these parameters and the regularization matrix $\mathbf{H}_1$ is of the form

$$\mathbf{H}_1 = \mathrm{diag}[1/\delta_i], \quad (33)$$

where δ_j represents the estimated standard deviation of an assumed Gaussian uncertainty distribution for the jth prior parameter estimate $\hat{m}_j$.

The second regularization term is optional, and can be used (when applicable) to apply the prior expectation that the array shape is expected to be a smooth function of position (x, y, z). This can be applied using $\hat{\mathbf{m}}_2 = \mathbf{0}$ and $\mathbf{H}_2$ consisting of a Toeplitz matrix with non-zero entries on jth row of the form

$$\mathbf{H}_{2j} = \left[0, \ldots, \frac{-1}{(u_{j+1} - u_j)^2}, \frac{u_{j+2} - u_j}{(u_{j+2} - u_{j+1})(u_{j+1} - u_j)^2}, \right.$$
$$\left. \frac{-1}{(u_{j+2} - u_{j+1})(u_{j+1} - u_j)}, \ldots, 0\right], \qquad (34)$$

applied to the x, y, and z receiver position variables, where u_j represents the distance along the array to the jth receiver. Each row of $\mathbf{H}_2$ in Eq. (34) represents a discrete approximation to the second derivative operator $\partial^2/\partial u^2$. Hence, $|\mathbf{H}_2\,\mathbf{m}|^2$ provides a measure of the total curvature of the array shape, and the regularization produces the simplest array shape that is consistent with the acoustic data and prior position estimates.

The regularized solution is obtained by setting $\partial\phi/\partial\mathbf{m} = 0$, leading to [3]

$$\mathbf{m} = \hat{\mathbf{m}}_1 + \left[\mathbf{J}^T\mathbf{G}^T\mathbf{G}\,\mathbf{J} + \mu_1\,\mathbf{H}_1^T\mathbf{H}_1 + \mu_2\,\mathbf{H}_2^T\mathbf{H}_2\right]^{-1} \left[\mathbf{J}^T\,\mathbf{G}^T\mathbf{G}\,\mathbf{d} - \mathbf{J}\hat{\mathbf{m}}_1\right]. \qquad (35)$$

AEL inversion consists of an iterative application of the regularized solution, typically initiated from a starting model coinciding with the prior parameter estimates. Convergence is based on achieving a statistically appropriate fit to the acoustic data (i.e., that the χ^2 misfit achieves its expected value of $\langle\chi^2\rangle = N$ for N data) and obtaining a stable solution such that the change in receiver locations between iterations is small compared to the desired accuracy. A practical aspect of implementing the inversion involves assigning values to the trade-off parameters, μ_1 and μ_2, which control the balance between the data misfit and the various forms of prior information; a straightforward procedure is described in [3].

An important component of any inverse problem is estimating the uncertainty of the solution. For linear problems with Gaussian-distributed data errors and prior estimates, the posterior model covariance matrix is given by

$$\mathbf{C} = [\mathbf{J}^T\mathbf{G}^T\mathbf{G}\,\mathbf{J} + \mathbf{H}_1^T\,\mathbf{H}_1]^{-1}, \qquad (36)$$

with the ith diagonal element of $\mathbf{C}$ representing the variance (standard deviation squared) of the ith recovered parameter. For nonlinear inverse problems solved via iterated linearized inversion, the covariance matrix can be approximated by Eq. (36) with $\mathbf{J}$ evaluated at the final model. The validity of this approach depends on the degree of nonlinearity of the inverse problem, but has been found to be a good approximation for AEL inversion [12] (considered further in the following section). Because of the computational efficiency of the linearized uncertainty estimates, they provide a convenient and effective way to characterize AEL inversion results, and can be applied in designing optimal AEL surveys (described in Section 5).

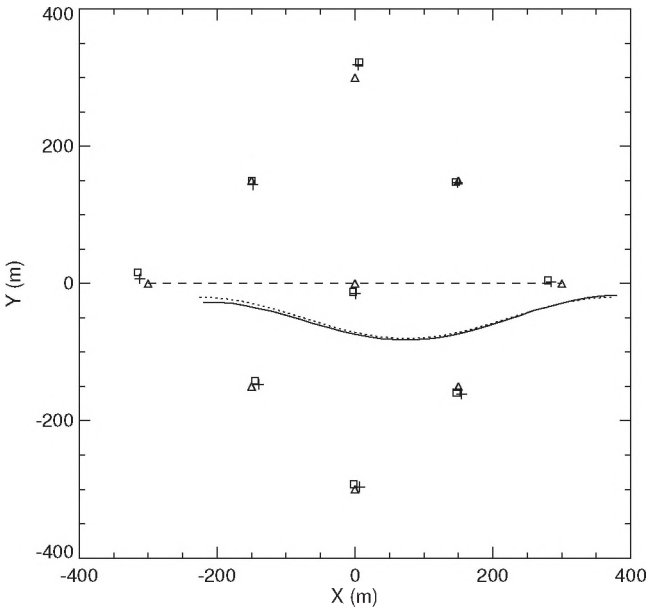

Figure 3: AEL inversion test case. The true position of the 31-element receiver array is indicated by the dotted line, the prior estimate by the dashed line, and the inversion result by the solid line. True positions, prior estimates, and inversion results for the source locations are indicated by the squares, triangles and crosses, respectively.

An example of the regularized AEL inversion is given in Fig. 3 for a synthetic test case based on a 600-m array of 31 equally spaced receivers (20-m separation) at approximately 75-m depth in a water-column with sound-speed profile shown in Fig. 2. As shown in Fig. 3, the starting model and prior estimate for the receiver locations consist of a straight array along the x axis from -300 to 300 m (dashed line), while the true array shape (dotted line) is curved and displaced by approximately 75 m in x and 50 m in y. The prior estimate for all receiver depths is 75 m, while the true depths include Gaussian-distributed random perturbations of 5-m standard deviation about this depth. The prior estimates for 9 source locations (triangles) are arranged symmetrically about the prior array estimate, with a 30-m source depth. The true source positions (squares) include random perturbations with standard deviations of 10 m in x and y and 3 m in z, corresponding to the assumed uncertainties of the prior estimates for these parameters (representative of measurements made at sea). Simulated AEL data (absolute travel times) were computed for direct-path arrivals and Gaussian errors of standard deviation 0.5 ms were added to produce the measured data set. AEL inversion was carried out for the smoothest array shape that fit the data and prior estimates to within their uncertainties. The inversion result for the receiver locations

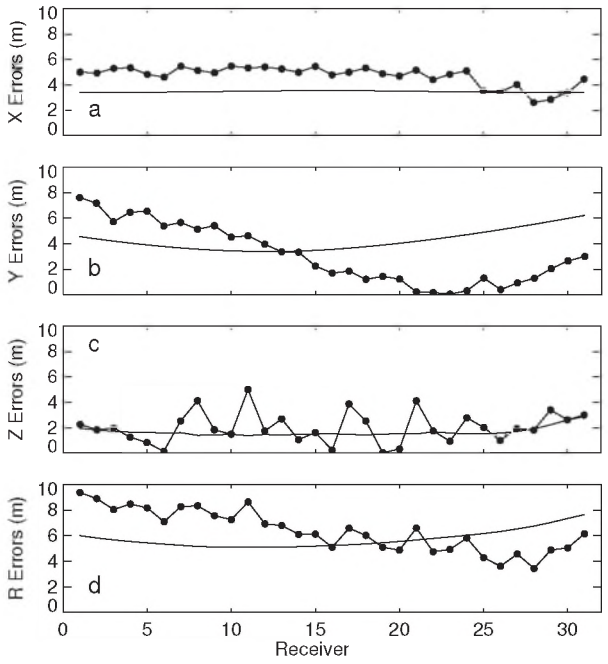

Figure 4: Localization errors for the AEL test case. Panels (a)–(d) show absolute errors (filled circles) and linearized uncertainty estimates (solid lines) for sensor locations in x, y, z, and R, respectively.

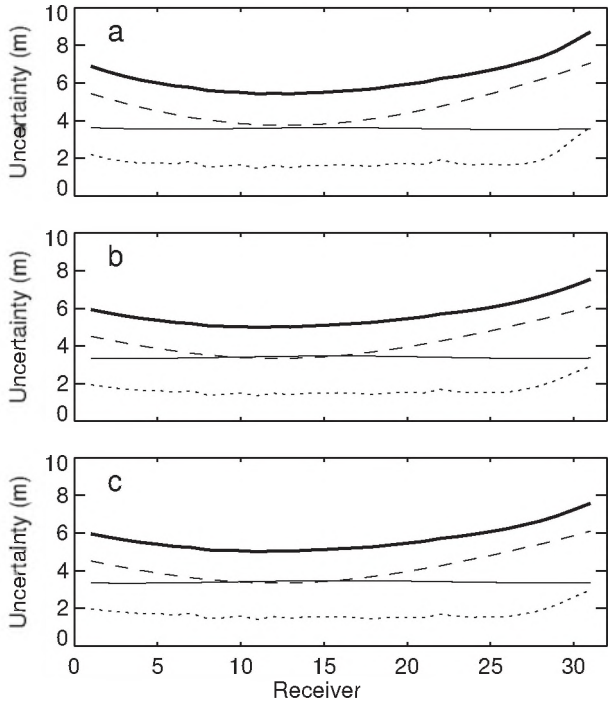

Figure 5: Linearized receiver-location uncertainties for relative travel-time data, absolute travel-time data, and absolute travel-time data with unknown offset shown in (a)–(c), respectively (uncertainties x, y, z, and R indicated by solid, dashed, dotted, and heavy solid lines).

(solid line) is in close agreement with the true receiver locations, although a small translation (to positive x) and rotation (counter-clockwise) is evident. The inversion results for the source locations (crosses) are generally significantly closer to the true source positions than to the prior estimates, particularly in cases where the true and prior locations differ substantially (e.g., at $x = \pm 300$ m and $y = +300$ m).

The AEL localization errors are examined in Fig. 4, which compares the absolute errors in x, y, z, and $R = [x^2 + y^2 + z^2]^{1/2}$ to the corresponding linearized posterior uncertainty estimates. The linearized uncertainties represent the actual errors reasonably well, although the results of the translation (in x) and rotation (in y) lead to some systematic differences (translations and rotations are specific to the particular data and prior errors, while the linearized estimates quantify expected uncertainties).

The effect of knowledge of source transmission instants is investigated in Fig. 5, in terms of linearized receiver position uncertainties in x, y, z, and R for the above AEL test case. The uncertainties for relative travel-time data (Fig. 5a), are slightly larger for all coordinates than the other two data types (Fig. 5b and c), with a total degradation of approximately 1 m in R. Figure 5(b) and (c) show virtually identical results for data consisting of absolute travel-times and absolute travel-times with an unknown offset.

The use of reflected arrivals in AEL is examined in Fig. 6, which compares the mean linearized receiver-location uncertainty in x, y, z, and R for five data sets consisting of different combinations of ray paths including: direct (d), surface-reflected (s), bottom-reflected (b), direct plus surface-reflected plus bottom-reflected (dsb), and all ray paths with up to one bottom reflection (all, six paths). The effect of water-depth uncertainty can be incorporated in the inversion by increasing the uncertainties of the bottom-reflected arrival-time data by an amount commensurate with propagation over the uncertainty in depth, as determined via ray-tracing. Water-depth uncertainties of 1, 3, and 8 m are considered in Fig. 6(a)–(c), respectively. Figure 6(a) shows that the receiver-location uncertainties in x and y are virtually unchanged by including reflected arrivals, as these follow identical radial paths and provide little new information regarding horizontal positioning. Compared to the direct-path inversion, the uncertainty in z is slightly improved for the surface-reflected path as it arrives at a steeper angle, but slightly degraded for the bottom-reflected path due the uncertainty in water depth. The localization uncertainty in z is significantly reduced by including multiple arrivals in the AEL inversion. Figure 6(a)–(c) show that the z localization uncertainties increase slightly with water-depth uncertainty for multiple-path inversions that include the bottom-reflected path, and increase significantly for the bottom-reflected only inversion. Figure 6(c) shows that inverting bottom-reflected data with large water-depth uncertainty leads to slightly degraded receiver-localization in x and y.

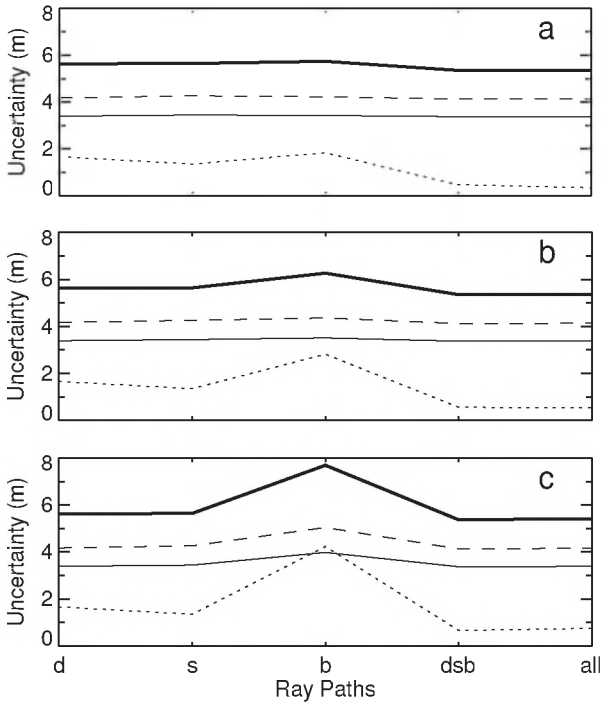

Figure 6: Mean linearized receiver-location uncertainties in x, y, z, and R (solid, dashed, dotted, and heavy solid lines, respectively) for different combinations of ray paths (defined in text). Panels (a)–(c) show results for water-depth uncertainties of 1, 3 and 8 m, respectively.

4. MONTE CARLO UNCERTAINTY ANALYSIS

The previous section described linearized uncertainty estimates which can be evaluated efficiently from the regularized solution. Monte Carlo appraisal provides an alternate approach which provides fully nonlinear uncertainty estimates, but is much more computationally intensive. In the Monte Carlo approach, the source and receiver positions determined via inversion of the measured data are assumed to define the true positions for a synthetic inverse problem, and acoustic arrival-time data are computed. A series of independent inversions are then carried out, each with different random errors applied to the computed data and to the prior position estimates and starting model (these errors are drawn from Gaussian distributions with standard deviations equivalent to the corresponding estimated uncertainties of the data and priors). Standard deviations about the true sensor positions can then be computed from the ensemble of inversion results.

An advantage of the Monte Carlo approach is that it can be used to estimate localization errors in both an absolute sense (relative to the fixed geographic coordinate system) and in a relative sense (in array-based coordinates), while linearized uncertainty estimates represent absolute errors. For some array processing applications, relative position errors provide a more relevant measure. This is because position errors common to all receivers are equivalent to a simple rigid-body translation and/or rotation of the receiver array. However, relative position errors introduce inter-receiver timing and phase errors which cannot be corrected by translation or rotation, and degrade applications such as matched-field localization.

To obtain relative error estimates from the Monte Carlo analysis, the effects of translations and rotations of the individual inversion estimates (relative to the true positions) are removed prior to computing the error statistics. Optimal estimates of these transformations are derived as follows. Let (x_i, y_i) represent N_r receiver-position estimates and (X_i, Y_i) represent the true positions. The optimal translation $(\delta x, \delta y)$ is found be minimizing the l_2 error norm (i.e., least-squares minimization)

$$E_1 = \sum_{i=1}^{N_r} \left\{ [x_i + \delta x - X_i]^2 + [y_i + \delta y - Y_i]^2 \right\}. \qquad (37)$$

Setting $\partial E_1/\partial \delta x = \partial E_1/\partial \delta y = 0$ yields

$$\delta x = \frac{1}{N_r} \sum_{i=1}^{N_r} [X_i - x_i] = \bar{X} - \bar{x}, \qquad (38)$$

$$\delta y = \frac{1}{N_r} \sum_{i=1}^{N_r} [Y_i - y_i] = \bar{Y} - \bar{y}, \qquad (39)$$

where the over-bar represents the mean over all receivers. Equations (38) and (39) indicate that the optimal translation consists of a shift in x and y equal to the difference between the mean true and estimated positions. To determine the optimal rotation (after translation), define rotated estimated positions as

$$\tilde{x}_i = r_i \cos(\theta_i + \psi), \qquad \tilde{y}_i = r_i \sin(\theta_i + \psi) \qquad (40)$$

where $r_i = [x_i^2 + y_i^2]^{1/2}$, $\theta_i = \tan^{-1}(y_i/x_i)$, and ψ is the rotation angle to be determined. The l_2 error norm between the rotated and reference positions is defined

$$E_2 = \sum_{i=1}^{N_r} \left\{ [r_i \cos(\theta_i + \psi) - X_i]^2 + [r_i \sin(\theta_i + \psi) - Y_i]^2 \right\}. \qquad (41)$$

Setting $\partial E_2/\partial \psi = 0$ for a minimum leads (after some algebra) to

$$\psi = \tan^{-1} \frac{\sum_i r_i (Y_i \cos\theta_i - X_i \sin\theta_i)}{\sum_i r_i (X_i \cos\theta_i - Y_i \sin\theta_i)}. \qquad (42)$$

As an example of the Monte Carlo appraisal, Fig. 7 compares both absolute and relative nonlinear receiver uncertainty estimates to the linearized uncertainty estimates derived in Section 3 for the AEL example considered previously. The regularized inversion and linearized uncertainty estimates required about 1–2 s computation time on a 2 GHz desktop computer running IDL (Interactive Data Language). The Monte Carlo uncertainties are based on 500 independent (randomized) inversions

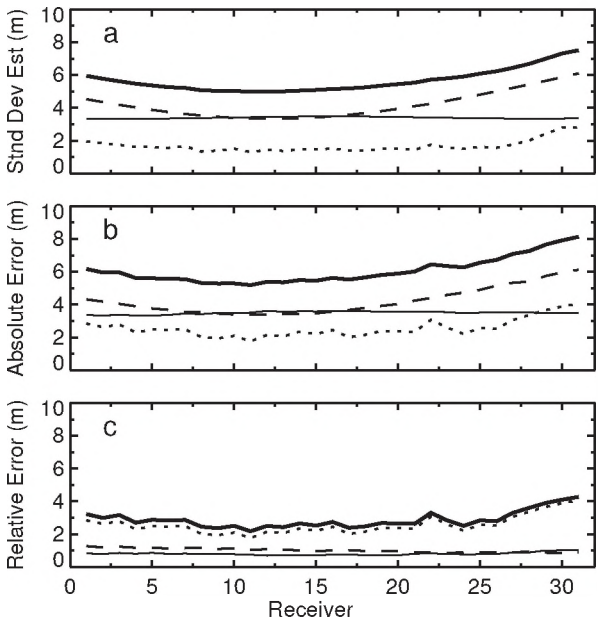

Figure 7: Receiver-location uncertainty estimates (uncertainties in x, y, z, and R indicated by solid, dotted, dashed, and heavy solid lines, respectively). Panel (a) shows the linearized uncertainty estimates (standard deviations), panels (b) and (c) show the absolute and relative uncertainties estimated by Monte Carlo appraisal.

which required about 15 minutes computation time. Figure 7(a) and (b) show that the linearized uncertainties and the Monte Carlo absolute uncertainties are in good agreement. Figure 7(c) shows that removing the effects of translation and rotation results in relative uncertainties that are substantially smaller in x, y, and R (not z). Finally, Fig. 8 shows that the relative errors from the AEL inversion (i.e., corrected for optimal translation and rotation) and the Monte Carlo relative uncertainty estimates are in excellent agreement.

5. OPTIMAL AEL SURVEY DESIGN

This section considers the problem of determining optimal AEL source configurations, i.e., the source configuration that produces the most accurate inversion for sensor positions. To this end, an AEL error measure is defined and the optimal survey configuration determined by minimizing this error with respect to the source positions [12]. Since this represents a difficult optimization problem which must be solved numerically, the AEL error must be computationally efficient, and hence is based on the linearized uncertainty estimates described in Section 3.

Let ξ_x, ξ_y, and ξ_z represent the standard deviations of the x, y, and z receiver-position coordinates as estimated by the square root of the diagonal elements of the linearized posterior covariance matrix given by Eq. (36).

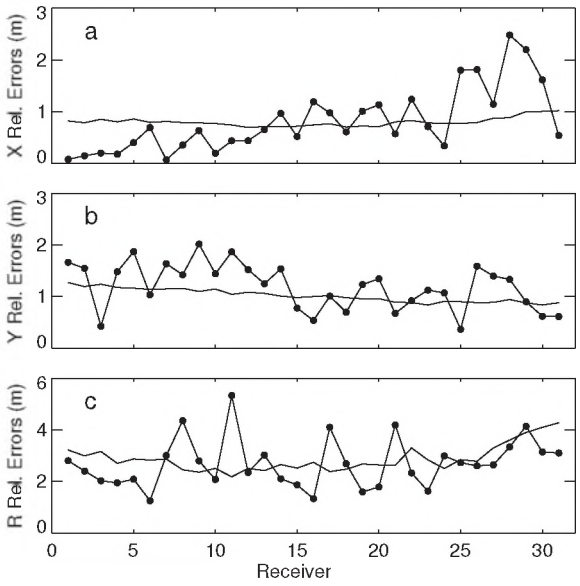

Figure 8: Relative receiver-location errors. Panels (a)–(c) show relative errors (filled circles) and Monte Carlo uncertainty estimates (solid lines) for sensor locations in x, y, and R, respectively.

The AEL error measure is then defined

$$E = \left[\frac{1}{N_s} \sum_{i=1}^{N_s} \xi_x^2 + \xi_y^2 + \xi_z^2 \right]^{1/2} . \qquad (43)$$

This measure represents the root-mean-square (RMS) 3-D uncertainty of the receiver positions. The source configuration that minimizes E provides the receiver-position estimates that are the most accurate on average.

Minimizing E in Eq. (43) represents a strongly nonlinear optimization problem that can have a degenerate global minimum (due to symmetries) and a large number of local minima, and hence is not amenable to linearized optimization methods. Here, an updated version of adaptive simplex simulated annealing (ASSA) is applied. ASSA represents an adaptive hybrid optimization that combines the local downhill simplex (DHS) method and very fast simulated annealing [17]. The version applied here included several advances over that described in [17]. First, the algorithm automatically determines an appropriate starting temperature based on the error functions associated with the models of the (randomly-chose) starting simplex. Second, multiple-contraction DHS steps are automatically applied in cases where the algorithm has difficulty finding improved solutions. Third, the adaptive component was modified to maintain a ratio of accepted to attempted perturbations of between 0.2–0.5 (the original version maintained a ratio of greater than 0.2). The modified version of ASSA appears to be significantly more efficient than the original.

To illustrate optimal AEL source configurations, consider first the configuration of 9 sources shown in Fig. 3: the expected RMS receiver error for this case is $E = 6.4$ m

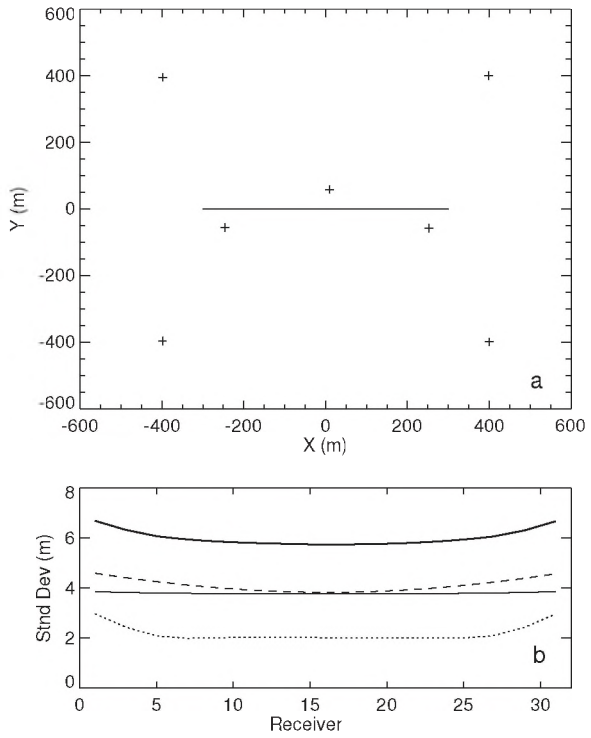

Figure 9: (a) Optimal configuration for 7 sources (crosses) to localize the receiver array (solid line). (b) Linearized standard deviation estimates for the optimal configuration (x, y, z, and R indicated by solid, dotted, dashed, and heavy solid lines, respectively)

(note that this applies for the prior straight-array estimate, since the true array shape is not known at the survey design stage). This error can be reduced significantly by using an optimal configuration for the AEL sources. In fact, the optimal configuration of just 7 sources (shown in Fig. 9), constrained within $-400 \leq x,\ y \leq 400$ m, leads to RMS error $E = 6.0$ m. The numerical optimization required approximately 15 minutes computation time.

The ability to compute optimal source configurations allows a variety of aspects of AEL survey design to be studied in an objective and meaningful manner. For instance, to examine the dependence of receiver localization error on the number of sources included in the AEL survey, it is only possible to separate the dependence on the number of sources from source-configuration effects by employing optimal source configurations. An example of such a study based on the the previously-described AEL test case (direct-arrival data) is given in Fig. 10. This figure shows the RMS receiver localization error as a function of the number of AEL sources (in optimal configurations) for the three types of data (absolute travel-times, relative travel-times, and absolute travel-times with unknown offset). The RMS localization uncertainties for data consisting of absolute travel-times with an unknown offset are virtually identical to those for absolute travel-times when more than three AEL sources

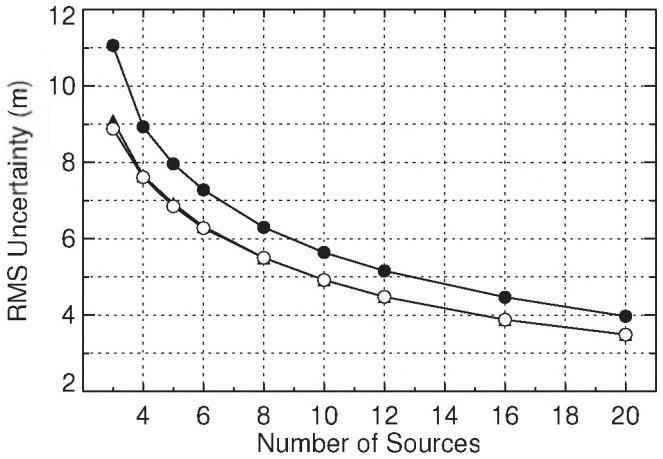

Figure 10: RMS receiver-location uncertainty versus number of sources for relative travel-time data (solid circles), absolute travel-time data (open circles), and absolute travel-time data with unknown offset (triangles, generally obscured by open circles). Data consist of direct arrival-times.

are employed (for three sources, the difference is 0.3 m). This indicates that little localization information is lost in solving for the unknown offset time. RMS uncertainties are always larger for relative travel-time data than for absolute travel-times, although the difference decreases with increasing number of sources (from about 2.3 m for three sources to ~0.5 m for 20 sources). Figure 10 shows that the advantages of using absolute travel-time data from synchronized surveys are relatively minor, and can be offset using relative travel times and an increased number of sources. For instance, Fig. 10 shows that using ten sources and relative travel-time data produces an RMS uncertainty equivalent to seven sources with absolute travel-time data.

The difference between localization errors for relative and absolute travel-time data can be also reduced

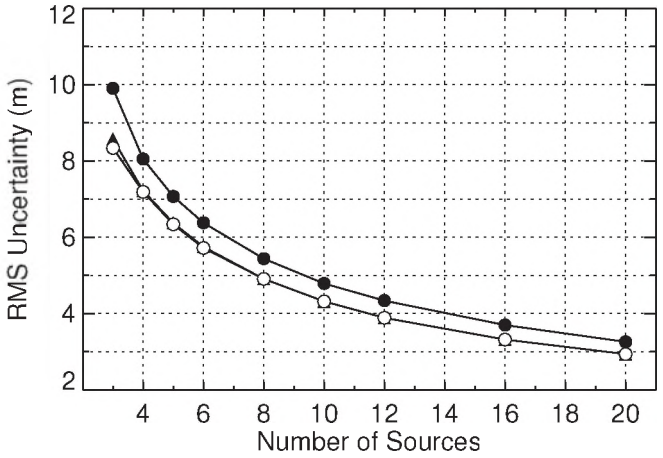

Figure 11: Same as Fig. 10, except data consist of direct and surface-reflected arrival-times.

by including reflected arrivals, since this provides additional data to constrain the same set of unknown source transmission instants. Figure 11 shows the RMS localization uncertainty for relative and absolute travel-time data including both direct and surface-reflected arrivals. This figure indicates that differences between the results for absolute and relative travel times are approximately half those in Fig. 10 for direct arrivals.

6. SUMMARY AND DISCUSSION

This paper presented the theory and implementation of a complete approach to AEL based on regularized inversion of the acoustic ray-tracing equations, which accounts for uncertainties in the data, source locations, sound speeds, and water depth. Posterior uncertainties in the recovered receiver locations are estimated efficiently from the linearized model covariance matrix, or from a fully nonlinear Monte Carlo appraisal at increased computational effort. The Monte Carlo analysis can also be applied to compute relative receiver-location uncertainties, which can be more relevant for some array-processing applications. The overall AEL error is quantified in terms of the RMS linearized receiver-location uncertainty, and optimal source configurations can be designed by minimizing this error measure over source positions via numerical optimization.

The ray-tracer developed here for AEL applications uses Newton's method to efficiently determine specific eigenrays to high precision without shooting a large number of rays to bracket the receiver. Surface and bottom reflections are included in this formulation using the method of images. Turning rays can also be included using a search based on rays that turn at sound-speed layer boundaries. The efficiency of the ray tracer and of the resulting AEL inversion algorithm allows computationally intensive analysis such as the Monte Carlo error estimation and nonlinear optimization for optimal source configurations.

The AEL algorithms developed here can be used to investigate factors affecting AEL accuracy and guide in designing AEL surveys. Several illustrations were given, including examining the relative advantages of synchronized versus non-synchronized AEL surveys and of including multi-path arrivals in AEL inversion. It is found that synchronized AEL surveys provide only a minor improvement over non-synchronized surveys, which can be made up by using more sources in an optimal configuration or by including reflected arrivals. AEL results based on absolute travel-time data with an unknown offset are virtually identical to absolute travel-time results. Including multiple-reflected arrivals can significantly improve receiver-depth estimation (if water depth is well known), but provides little improvement in horizontal localization as the rays follow identical radial paths.

ACKNOWLEDGEMENTS

The first author would like to thank several collaborators from earlier AEL projects in which many of the ideas described here originated, including Nicole Collison, Garry Heard, and Barbara Sotirin.

7. REFERENCES

[1] B. D. Steinberg, *Principles of Aperture and Array System Design* (Wiley, New York, 1976).

[2] P. H. Milne, *Underwater Acoustic Positioning Systems* (Cambridge Univ. Press, Cambridge, 1983).

[3] S. E. Dosso, M. R. Fallat, B. J. Sotirin, and J. L. Newton, "Array element localization for horizontal arrays via Occam's inversion," J. Acoust. Soc. Am. **104**, 846–859 (1998).

[4] M. Barlee, S. E. Dosso and P. Schey, "Array element inversion for a bottom-moored hydrophone array," Canadian Acoustics, **30**, 3–12 (2002).

[5] S. E. Dosso, N. E. Collison, G. J. Heard and R. I. Verrall, "Experimental validation of regularized array element localization," J. Acoust. Soc. Am., **115**, 2129–2137 (2004).

[6] S. E. Dosso, G. H. Brooke, S. J. Kilistoff, B. J. Sotirin, V. K. McDonald, M. R. Fallat, and N. E. Collison, "High-precision array element localization of vertical line arrays in the Arctic Ocean," IEEE J. Oceanic Eng., **23**, 365–379 (1998).

[7] S. E. Dosso and M. Riedel, "Array element localization for towed marine seismic arrays," J. Acoust. Soc. Am. **110**, 955–966 (2001).

[8] S. E. Dosso and N. E. Collison, "Regularized inversion for towed-array shape estimation," *Inverse Problems in Underwater Acoustics*, Edited by: M. Taroudakis and G. Makrakis, (Springer-Verlag, Berlin, 2001).

[9] S. E. Dosso and N. E. B. Collison, "Acoustic tracking of a freely drifting sonobuoy field," J. Acoust. Soc. Am., **111**, 2166–2177 (2002).

[10] N. E. Collison and S. E. Dosso, "Acoustic tracking of a freely-drifting sonobuoy field: Experimental results," IEEE J. Oceanic Eng., **28**, 554–561 (2003).

[11] H. T. Vincent II and S.-L. J. Hu, "Geodetic position estimation of underwater acoustic sensors," J. Acoust. Soc. Am. **102**, 3099 (1998).

[12] S. E. Dosso and B. J. Sotirin, "Optimal array element localization," J. Acoust. Soc. Am. **106**, 3445–3459 (2000).

[13] W. M. Telford, L. P. Geldart, R. E. Sheriff, and D. A. Keys, *Applied Geophysics* (Cambridge Univ. Press, New York, 1976).

[14] S. C. Constable, R. L. Parker, and C. G. Constable, "Occam's inversion: A practical algorithm for generating smooth models from electromagnetic sounding data," Geophysics **52**, 289–300 (1987).

[15] C. van Schooneveld, "Inverse problems: A tutorial survey," in *Underwater Acoustic Data Processing*, edited by Y. T. Chan, (Kluwer, The Netherlands, 1989) pp. 393-411.

[16] J. A. Scales, P. Docherty, and A. Gersztenkorn, "Regularisation of nonlinear inverse problems: Imaging the near-surface weathering layer," Inverse Problems **6**, 115–131 (1990).

[17] S. E. Dosso, M. J. Wilmut and A. L. Lapinski, "An adaptive hybrid algorithm for geoacoustic inversion," IEEE J. Oceanic Eng., **26**, 324–336 (2001).

Noise Pollution

The SLARM™ Solution

The **SLARM**™ developed in response to increased emphasis on hearing conservation and comfort in the community and workplace incorporates **ACOustAlert**™ and **ACOustAlarm**™ technology. Making the **SLARM**™ a powerful and versatile sound monitoring/alarm system.

Typical Applications Include:

Community

- Amphitheaters
- Outdoor Events
- Nightclubs/Discos
- Churches
- Classrooms

Industrial

- Machine/Plant Noise
- Fault Detection
- Marshalling Yards
- Construction Sites
- Product Testing

FEATURES

- √ Wired and Wireless (opt)
- √ USB, Serial, and LAN(opt) Connectivity
- √ Remote Display s and Programming
- √ SPL, Leq, Thresholds, Alert and Alarm
- √ Filters (A,C,Z), Thresholds, Calibration
- √ Multiple Profiles (opt)
- √ 100 dB Display Range:
- √ 20-120 dBSPL and 40-140 dBSPL
- √ Real-time Clock/Calendar
- √ Internal Storage: 10+days @1/sec
- √ Remote Storage of 1/8 second events
- √ 7052S Type 1.5™ Titanium Measurement Mic

ACO Pacific

2604 Read Ave., Belmont, CA 94002 Tel: 650-595-8588 FAX: 650-591-2891
www.acopacific.com acopac@acopacific.com

ACOustics Begins With ACO™